

Level scheme of ^{114}Sb from the $(p, n\gamma)$ reaction

Z. Gácsi and Zs. Dombrádi

Institute of Nuclear Research, P.O.B. 51, 4001 Debrecen, Hungary

(Received 25 April 1994)

Measurement of γ , $\gamma\gamma$ -coincidence, internal conversion electron and γ -ray angular distribution spectra for the $^{114}\text{Sn}(p, n\gamma)^{114}\text{Sb}$ reaction were made at 7.8 and 8.0 MeV bombarding proton energies with Ge γ -ray and superconducting magnetic lens-plus-Si(Li) electron spectrometers. The energies and relative intensities of 74 ^{114}Sb γ rays, as well as the internal conversion coefficients of 31 ^{114}Sb transitions have been determined and new angular distribution data have been obtained for 26 γ rays. From this information, a more complete and consistent level scheme has been deduced. Spin and parity values have been determined from the internal conversion coefficients, Hauser-Feshbach analysis of the (p, n) reaction cross sections, and the γ -ray angular distributions. The low-lying levels were grouped into proton-neutron multiplets and the energy splitting of these multiplets have been interpreted in terms of the parabolic rule.

PACS number(s): 23.20.Lv, 23.20.En, 27.60.+j, 25.40.Kv

I. INTRODUCTION

The structure of ^{114}Sb nucleus was studied from $^{114}\text{Te} \rightarrow ^{114}\text{Sb}$ decay by Wigmans *et al.* [1], and in (p, n) reaction by Kamermans *et al.* [2]. Van Nes *et al.* [3] and Duffait *et al.* [4] explored the states of higher spin (>6). The 8^- , 219 μs isomeric state was studied by Gil *et al.* [5], and the magnetic dipole moment of the ground state was measured by Zimmerman *et al.* [6]. Data on the ^{114}Sb nucleus were last compiled in 1990 [7].

As a result of these works, accurate γ -ray energy values are available, but due to the lack of low-energy transitions in the published data, the position of many transitions in the level scheme seems to be unreliable. Furthermore, if one examines the systematic behavior of the low-lying states in the odd- A tin and antimony nuclei, a set of 6–8 closely spaced states is expected to appear near the ground state [8], and there has been no mention of such a phenomenon in ^{114}Sb . More importantly, in-beam conversion electron spectra have not been measured for transitions between low-spin states and definite spin and parity values below 1 MeV excitation energy are known only for the ground and the isomeric states.

To interpret the data previously available on the level structure of ^{114}Sb , van Gunsteren *et al.* [8] used a particle-quasiparticle model. The agreement of their theoretical results with our experimental data is not good.

II. EXPERIMENTAL TECHNIQUES

The present nuclear spectroscopic experiments have been performed at the Debrecen 103-cm isochronous cyclotron. We used self-supporting, 0.4–2.5 mg/cm² thick ^{114}Sn targets, which were prepared by an evaporation technique from isotopically enriched (to 70%) metal powder. For reliable identification of γ rays, we also studied the $^{116,117,118,119,120}\text{Sn}+p$ reactions.

The targets were bombarded with 30–900 nA proton beams at $E_p=7.8$ and 8.0 MeV energies. The γ -ray spectra were measured with 20% and 25% Ge(HP) detectors, and with a 2000 \times 13 mm³ planar Ge(HP) low-energy photon spectrometer (LEPS). The detectors were placed at 90° to the beam direction for energy determination and at 125° for intensity measurements. The energy resolutions of the detectors were ≈ 2 keV (at 1332 keV) and ≈ 0.8 keV (at 122 keV), respectively.

For energy and efficiency calibration of the γ spectrometers ^{133}Ba and ^{152}Eu sources were used. Using this energy calibration, the energies of the strong 887.60(5) and 1299.90(8) keV ^{114}Sn [7] internal calibration lines have been reproduced within experimental uncertainties.

Internal conversion electron spectra were measured with a superconducting magnetic lens spectrometer (SMLS) with Si(Li) detectors [9]. The energy resolution and transmission of the SMLS were ≈ 2.7 keV (at 946 keV) and $\approx 10\%$ (for two detectors), respectively. The background from backscattered electrons was reduced with a swept energy window in the spectrum of the Si(Li) detector. Further background reduction was achieved by using paddle-wheel-shaped antipositron baffles. For the calibration of the spectrometer, ^{133}Ba , ^{152}Eu , and ^{207}Bi sources were used.

The γ -ray and internal conversion electron intensities were normalized by using the internal conversion coefficients of the strongest ^{116}Sb transitions [10], since the target contained more than 9% of ^{116}Sn isotope.

The angular distributions of the γ rays were measured at 8.0 MeV proton bombarding energy at 12 angles with respect to the beam direction ranging from 90° to 145° in 5° steps. The solid angle correction factors were $Q_2=0.983$ and $Q_4=0.945$. For the normalization of the spectra, we used the 93-keV ^{116}Sb γ ray, which has an isotropic distribution (the half-life of the 93-keV isomeric level is more than 200 ns [11]).

The theoretical angular distributions for different spin

combinations were fitted to the experimental data in a least-squares procedure using the computer code ANDIST [12]. The attenuation coefficients α_2 and α_4 were calculated with the CINDY [13] program. The effect on the alignment of the γ -ray feeding to the levels was also considered. The optical potential parameters used in the calculations are given in Sec. IV A.

The effect of the angular distribution of the conversion electrons on the measured internal conversion coefficients was estimated using the γ -ray angular distribution coefficients, the solid angle correction factors, and the normalized directional particle parameters. It was found that this effect is much smaller than the statistical uncertainty of the conversion coefficients.

The $\gamma\gamma$ -coincidence data were acquired at 8.0 MeV bombarding proton energy, with a fixed $\tau=80$ ns resolving time. The 20% and 25% Ge(HP) detectors were placed at 125° and 235° angles to the beam direction. Approximately 41×10^6 $\gamma\gamma$ -coincidence events were recorded on magnetic tapes in event-by-event mode for subsequent analysis. To get more information on the coincidence relations of the low-energy gamma rays, a second coincidence measurement was performed, using the 20% Ge(HP) and the LEPS detectors. In this experiment a proton beam with 7.8 MeV energy was used and the detectors were placed at 125° and 90° angles to the beam direction, respectively. About 21×10^6 $\gamma\gamma$ -coincidence events were recorded on magnetic tapes in this case. After creating the symmetrized, two-parameter coincidence matrices, a standard gating procedure was applied.

All measurements were performed with CAMAC modular units connected to a TPA 11/440 computer and to multichannel analyzer cards mounted in personal computers. The data reduction was carried out using a γ -spectrum [14] analyzing program.

III. EXPERIMENTAL RESULTS

Typical γ -ray and internal conversion electron spectra are shown in Fig. 1. The γ -spectrum measurement of the $^{114,116,117,118,119,120}\text{Sn}+p$ reactions (at $E_p=7.8$ and 8.0 MeV) and the study of the radioactive decay of the reaction products enabled unambiguous γ -ray identification in most cases. The energies and relative intensities of the γ rays assigned to ^{114}Sb are listed in Table I, together with their internal conversion coefficients, multiplicities, and coincidence relations.

The internal conversion coefficients of ^{114}Sb transitions and typical $\gamma\gamma$ -coincidence spectra are shown in Fig. 2 and in Fig. 3, respectively.

The results of the angular distribution measurements are summarized in Table II. The angular distribution of the 209-keV and 264-keV γ rays are displayed in Fig. 4. The reduced χ^2 fits of the theoretical distribution to the experimental ones are also shown. It is clearly seen how the spin of the 54-keV level could be pinned down. In general, only spin, parity, and multipole-mixing-ratio values allowed by the internal conversion coefficient measurements were considered in the angular-distribution

fits. Spins were rejected on the basis of a 0.1% confidence limit for the reduced χ^2 fits. The uncertainty of the mixing ratios (δ) corresponds to the $\chi^2_{\min} + 1$ values.

IV. LEVEL SCHEME OF ^{114}Sb

The level scheme obtained from the $^{114}\text{Sn}(p, n\gamma)$ reaction was constructed mainly on the basis of $\gamma\gamma$ -coincidence results, but the energy and intensity balance of transitions was also taken into account. Moreover, the multipolarity of transitions allowed us to separate positive- and negative-parity levels. In this way, two levels lying only 0.07 keV apart at 665 keV could be resolved and identified. The proposed level scheme is displayed in Fig. 5.

A new level at 27.4 keV is introduced. Its existence has been deduced from the fact, among others, that the intensity ratio of the 56-keV and 84-keV γ rays in singles spectra agrees with the ratio obtained in the gate spectra where they are observed. Consequently, they decay from the same level. A similar statement is true for the 188-keV and 244-keV transitions. In this manner, the 27-keV level energy is readily arrived at. Direct evidence could not be obtained, since the 27-keV γ ray is a mixture of x rays and at least one other transition and at such a low energy, the internal conversion electrons carry away the majority of transition strength hindering any γ -ray detection.

The new level at 45.9 keV is established by coincidence relations between the 45-keV and 299-keV γ rays. The 299-keV γ ray decays from the 344-keV level as verified in the gate spectrum of the 147-keV γ ray. Similarly, the 455-keV γ ray decays into the 46-keV level from the 501-keV level as indicated by the gate spectrum of the 163-keV γ ray.

The 55-keV level is based mainly on the coincidence relations between the 55-keV and 90-keV γ rays and the 55-keV and 210-keV γ rays, as well as the 55-keV and 636-keV γ rays. The 210-keV γ ray decays from the 264-keV level as indicated by the gate spectra of the 80-keV and 147-keV γ rays.

The 56-keV level is removed because of placing the 56-keV γ ray as a decay from the 83.9-keV level.

In the vicinity of the 83.9-keV level another new level is introduced at 83.4 keV determined by the 181-keV γ ray, which is placed as a decay from the 264-keV level according to its coincidence relations. The previously observed [3] coincidence relation between the 37–45-keV γ rays is also consistent with this level. A decay to the ground state is expected in order to have a reasonable intensity balance. Such an 83.4-keV γ ray was not separated from the very strong 83.9-keV γ ray, but cannot be ruled out.

The previously claimed 90.3-keV level [7] is removed now because the order in the cascade of the 55-keV and 90-keV γ rays as well as the 46-keV and 90-keV γ rays has been reversed based on the present coincidence relations (especially the information in the gate spectra of 347-keV, 519-keV, 664-keV, and 727-keV γ rays) and transition intensity ratios. The presence of both the 55-keV and 46-keV γ rays in the 90-keV gate suggests an

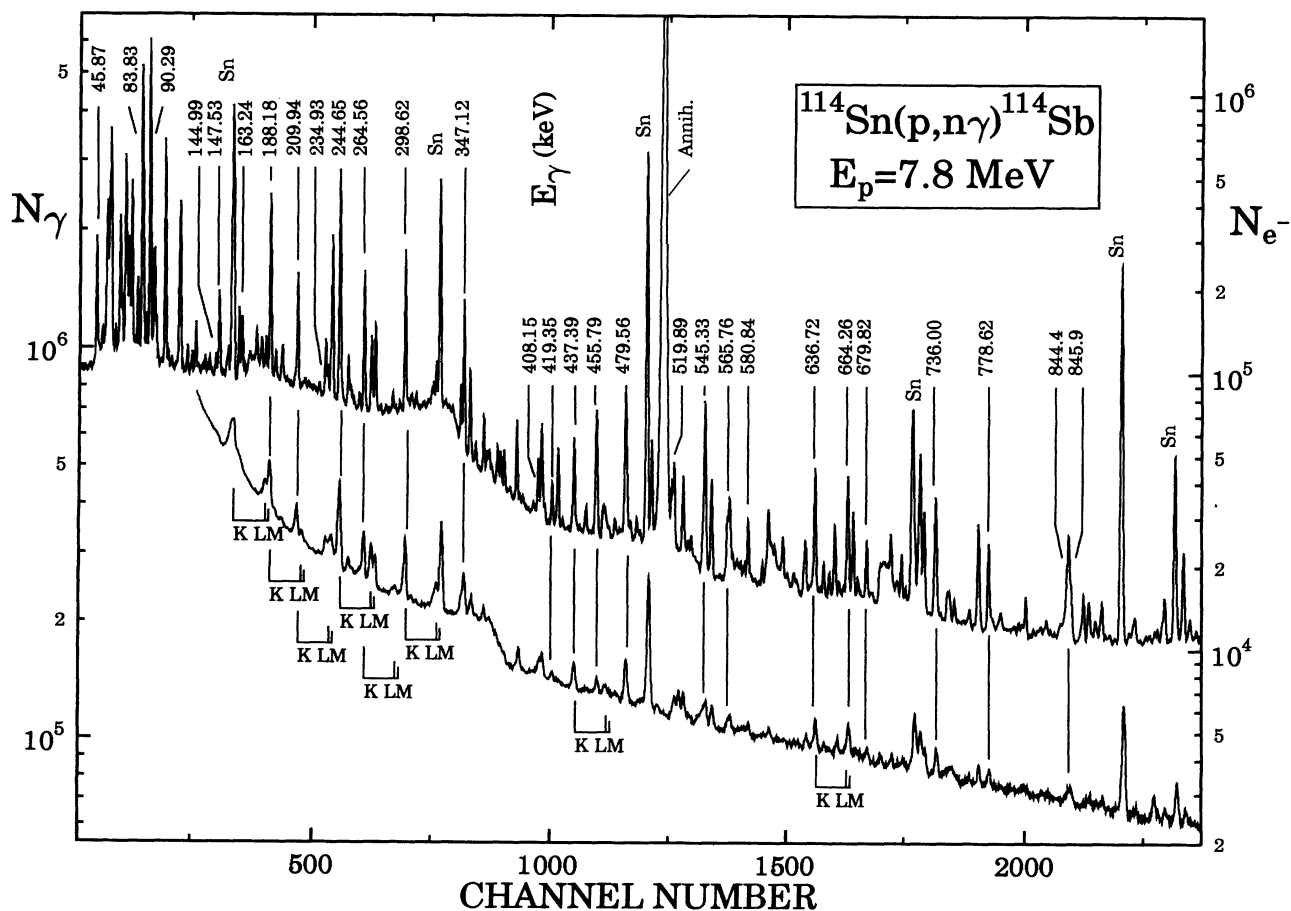


FIG. 1. Typical γ -ray and internal conversion electron spectra of the $^{114}\text{Sn}(p, n\gamma)^{114}\text{Sb}$ reaction. K, L, M denote conversion electron lines.

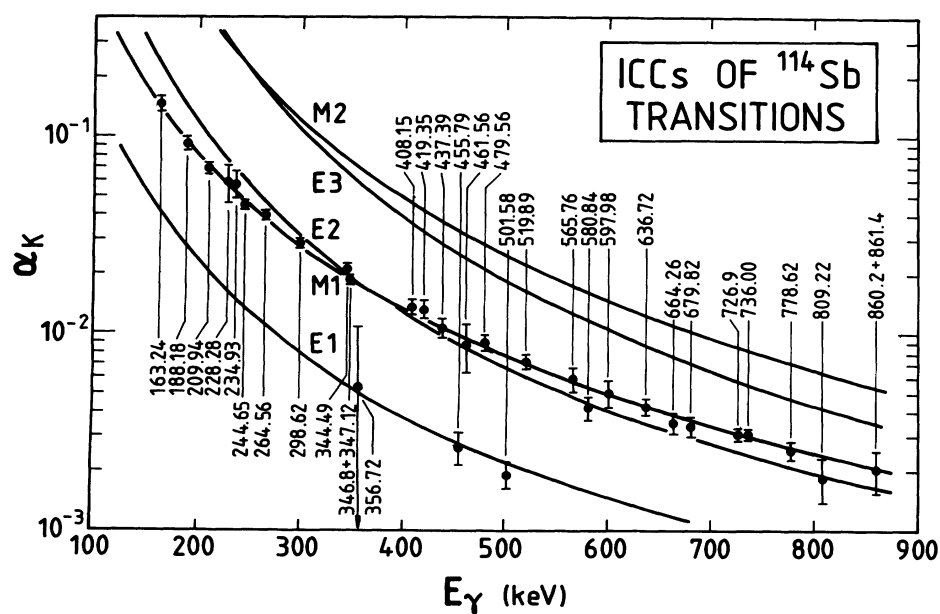


FIG. 2. The internal conversion coefficients of ^{114}Sb transitions.

TABLE I. The energy (E_γ) and relative intensity (I_γ) of γ rays observed in the $^{114}\text{Sn}(p, n\gamma)^{114}\text{Sb}$ reaction at $E_p=8.0$ MeV. Internal conversion coefficients, multipolarities, and coincidence relations are also given.

E_γ (keV)	I_γ (relative)		ICC measurement		Coincident γ rays (keV)
			$\alpha_k \times 10^3$	Multipol.	
27.5(3)	240(100) ^a	S ^b			
37.4(4)	weak	S			
45.87(3)	293(17)	S			90, 299
54.65(3)	340(18)	S			90, 210, 346.8, 437, 519, 637, 727, (751) ^c
56.3(2)	16(8)	S			188, (581), 680, 722
79.94(2)	96(3)	S			55, 148, 181, 210, 265, 462
83.83(2)	831(29)	S			188, 235, (301), 380, 408, 419, 534, 581, 598, 680, 719, 722, 746, 861, 934
90.29(2)	1000(35)	S			46, 55, 163, 272, 347, 357, 380, 520, 619, 664, 727, 800, 846, 860
92.3(2)	23(3)				
144.99(3)	21.3(11)	S			(347)
147.53(2)	124(6)	S			80, 210, 265, 272, 299, 344, 380
163.24(3)	108(6)	S	146(12)	$M1, (E2)$	90, 228, 357, 456, 502
181.15(3)	41.7(24)	S			80, 148, 377
188.18(2)	423(25)	S	92(7)	$M1, (E2)$	56, 84, 235, (301), 419, 534, 598, 719, 746
209.94(2)	217(10)	S	69(4)	$M1, (E2)$	55, 80, 148, 346.8, 377, 462, 529, 544, (684)
218.8(3)	5.1(10)	(S)			
228.28(4)	17.0(9)	S	59(13)	$M1, E2$	163, 456, (502)
234.93(3)	47.7(24)	S	58(9)	$M1, E2$	84, 188, 245
244.65(2)	684(24)	S	44.9(25)	$M1, (E2)$	235, 301, 419, 534, 598, 719, 746
256.6(3)	12.6(5)	S			480
264.56(2)	310(11)	S	40.1(25)	$M1, E2$	80, 148, 347, 377, 462, 529, 544, 601, 684
271.8(5)	32(10)	S			90, 148, 347
298.62(2)	422(13)	S	28.7(16)	$M1, E2$	46, 148, 320, 346.8, 380, 462, 464, 601, (672)
301.0(3)	20(3)	S			(188), 245
320.4(2)	29.0(12)	S			299
344.49(2)	113(26)	S	21.1(14)	$M1, E2$	148
346.8(5)	368(9)	S	18.7(10)		80, 210, 265, 299, 344
347.12(6)		S			55, 90, 145, 272, 380, (453)
356.72(9)	29.2(8)	S	5.4(55)	$E1$	90, 163
365.68(5)	5.22(14)				
376.93(5)	55.2(22)	S			181, 210, 265
379.93(6)	59.9(16)	S			55, 84, 90, 148, 299, 347, 408, 437
392.8(3)	12(3)				
408.15(2)	86.7(24)	S	13.6(12)	$M1, (E2)$	84, 380
419.35(3)	55.6(16)	S	13.1(12)	$M1, (E2)$	84, 188, 245
437.39(3)	157(5)	S	10.6(12)	$M1, E2$	55, 272, 380
453.4(3)	3.3(8)	S			
455.79(2)	236(7)	S	2.6(5)	$E1$	163, 228
461.56(10)	43.6(24)	S	8.7(24)	$M1, E2$	80, 210, 265, 299, 344
464.6(3)	19.3(12)	S			
479.56(3)	315(13)	S	9.0(8)	$M1, (E2)$	257, 484
483.78(22)	24.1(9)	S			480
501.58(3)	182(6)	S	1.9(3)	$E1$	163
519.89(3)	135(10)	S	7.2(6)	$M1, (E2)$	55, 90
528.8(4)	12(4)	S			210, 265
534.03(14)	30.6(11)	S			84, 188, 245
544.3(5)	42.3(15)	S			210, 265
545.33(3)	362(14)	S			
565.76(3)	127(9)	S	5.9(8)	$M1, E2$	
580.84(5)	94(4)	S	4.2(6)	$(M1), E2$	56, 84
597.98(12)	80(12)	S	5.0(9)	$M1, E2$	84, 188, 245
600.7(5)	15(6)	S			265, 299
618.9(5)	15(7)	S			
636.72(3)	248(10)	S	4.3(4)	$M1, (E2)$	55
664.26(4)	253(11)	S,D	3.5(4)		90
672.40(16)	20.9(10)				(299)

TABLE I. (Continued).

E_γ (keV)	I_γ (relative)		ICC measurement		Coincident γ rays (keV)
			$\alpha_k \times 10^3$	Multipol.	
679.82(4)	95(4)	S	3.4(4)	$M1, E2$	84
684.15(20)	8.8(12)	S			210, 265
718.8(9)	60(40) ^a	S			84, 188, 245
722.14(7)	100(8)	S			84
726.9(1)	200(6)	S	3.06(23)	$M1, (E2)$	55, 90, 145
736.00(9)	234(9)	S	3.07(22)	$M1, (E2)$	
745.7(4)	38.7(14)	S			
751.4(3)	30(4)	S			
778.62(5)	152(5)	S	2.5(3)	$M1, E2$	
800.3(4)	10.0(19)	S			
806.2(3)	16.5(8)	S			
809.22(7)	59.6(22)	S	1.8(5)	$M1, E2$	
842.5(5)	79(6)	S			
844.4(5)	56(14)	S			
845.9(5)	56(23)	S			55, 90
860.2(5)	59.2(23)	S	2.0(5)		90
861.4(5)		S			84
933.8(3)		S			84

^aEstimated intensity.^bS, placed in scheme; D, doubly placed.^cWeak coincidence in parentheses.TABLE II. Results of the gamma-ray angular distribution measurements from the $^{114}\text{Sn}(p, n\gamma)^{114}\text{Sb}$ reaction performed at $E_p=8.0$ MeV. Delta values are marked by an asterisk, if the spin combination is rejected by the high χ^2 value, or the mixing ratio (δ) obtained for a stretched $E2$ transition is a finite value within its uncertainty. The uncertainty of the mixing ratio is given for the accepted spin combination.

E_i (keV)	E_f (keV)	E_γ (keV)	Multipol. from ICC	Angular distribution coefficients		J_i^π	J_f^π	δ
				A_2	A_4			
54.64	0	54.65		0.16(18)	-0.20(27)	1 ⁺	3 ⁺	*
						2 ⁺		-0.84
						3 ⁺		$0.05^{+0.18}_{-0.14}$
						4 ⁺		0.38
						5 ⁺		*
83.85	0	83.83		0.040(18)	0.034(22)	1 ⁺	3 ⁺	*
						2 ⁺		-0.12(5)
						3 ⁺		-0.40
						4 ⁺		0.18
						5 ⁺		*
144.9	54.64	90.29		0.027(17)	0.039(20)	2 ⁺	0 ⁺	*
							1 ⁺	-8.14
							2 ⁺	-0.32
							3 ⁺	-0.11(6)
							4 ⁺	*
264.56	0	264.56	$M1, E2$	-0.25(4)	0.05(6)	1 ⁺	3 ⁺	*
						2 ⁺		0.81
						3 ⁺		-1.66
						4 ⁺		-0.02(5)
						5 ⁺		*
272.03	54.64	209.94	$M1, (E2)$	-0.19(3)	0.07(4)	4 ⁺	3 ⁺	0.00(4)
							4 ⁺	*
							5 ⁺	0.09
							1 ⁺	0.00
							1 ⁺	$0.14^{+\infty}_{-0.46}$
83.85	27.4	244.65	$M1, (E2)$	0.13(5)	0.11(6)	1 ⁺	0 ⁺	0.00
							1 ⁺	$0.14^{+\infty}_{-0.46}$
							2 ⁺	-0.7
							0 ⁺	0.00
							1 ⁺	-0.19
	83.85	188.18	$M1, (E2)$	0.01(3)	0.02(4)	1 ⁺	0 ⁺	0.00
						1 ⁺		-0.19
						2 ⁺		$-0.03^{+\infty}_{-\infty}$

TABLE II. (Continued).

E_i (keV)	E_f (keV)	E_γ (keV)	Multipol. from ICC	Angular distribution coefficients		J_i^π	J_f^π	δ
				A_2	A_4			
344.49	0	344.49	$M1, E2$	0.35(9)	0.22(10)	1 ⁺	3 ⁺	*
						2 ⁺		-0.84
						3 ⁺		-0.09(20)
						4 ⁺		4.33
						5 ⁺		*
	45.85	298.62	$M1, E2$	0.02(4)	-0.01(5)	3 ⁺	1 ⁺	*
							2 ⁺	0.22
							3 ⁺	-0.40
							4 ⁺	-0.13(7)
							5 ⁺	0.16
492.01	54.64	437.39	$M1, E2$	0.04(8)	0.08(9)	1 ⁺	3 ⁺	2.47
						2 ⁺		-0.08(22)
						3 ⁺		-0.47
						4 ⁺		0.16
						5 ⁺		*
	83.85	408.15	$M1, (E2)$	0.07(5)	0.04(6)	2 ⁺	1 ⁺	0.28
							2 ⁺	-0.24 ^{+0.12} _{-0.14}
							3 ⁺	-0.19
							2 ⁺	*
							1 ⁺	*
	144.94	347.12		0.23(5)	0.12(6)	0 ⁺	2 ⁺	*
						1 ⁺		*
						2 ⁺		-0.02 ^{+0.10} _{-0.13}
						3 ⁺		8.14
						4 ⁺		*
501.63	0	501.58	$E1$	0.39(5)	0.00(7)	2 ⁻	3 ⁺	*
						3 ⁻		0.18 ^{+0.22} _{-0.13}
						4 ⁻		0.47
						3 ⁻	2 ⁺	0.11
							3 ⁺	-0.67
	45.85	455.79	$E1$	-0.11(3)	-0.01(4)		4 ⁺	0.00(5)
							2 ⁺	1.33
							2 ⁻	-1.54
							3 ⁻	-0.07(18)
							0 ⁺	0.00
506.96	27.4	479.56	$M1, (E2)$	0.12(10)	0.18(13)	0 ⁺	1 ⁺	0.00
	272.03	234.93	$M1, E2$	-0.04(9)	0.04(12)	0 ⁺	1 ⁺	0.00
565.76	0	565.76	$M1, E2$	-0.22(8)	0.07(11)	1 ⁺	3 ⁺	2.14
						2 ⁺		0.39
						3 ⁺		-1.23
						4 ⁺		0.00(9)
						5 ⁺		*
572.7	27.4	545.33		-0.18(5)	-0.03(6)	1 ⁺	0 ⁺	*
						1 ⁺		-1.00
						2 ⁺		0.02(9)
						3 ⁺		-0.91
641.49	264.56	376.93		0.02(20)	0.55(23)	2 ⁺	4 ⁺	11.5
						3 ⁺		0.18
						4 ⁺		-0.97
						5 ⁺		-0.01(20)
						6 ⁺		*
664.80	501.63	163.24	$M1, (E2)$	-0.31(13)	-0.21(17)	2 ⁻	3 ⁻	0.21
						3 ⁻		-5.67
						4 ⁻		0.05(13)
664.87	144.94	519.89	$M1, (E2)$	-0.39(11)	0.01(14)	1 ⁺	2 ⁺	*
						2 ⁺		-1.48
						3 ⁺		-0.09(14)
691.37	54.64	636.72	$M1, (E2)$	0.13(10)	0.23(12)	2 ⁺	1 ⁺	-8.14
							2 ⁺	-0.32
							3 ⁺	-0.11 ^{+0.28} _{-0.41}
	272.03	419.35	$M1, (E2)$	-0.18(10)	0.08(13)	2 ⁺	1 ⁺	-0.03 ^{+0.19} _{-0.24}
							2 ⁺	-1.07
							3 ⁺	0.28

TABLE II. (Continued).

E_i (keV)	E_f (keV)	E_γ (keV)	Multipol. from ICC	Angular distribution coefficients		J_i^π	J_f^π	δ
				A_2	A_4			
806.0	27.4	778.6	$M1, E2$	-0.31(5)	-0.05(5)	2^+	3^+ 0^+ 1^+ 2^+ 3^+ 4^+	0.28 * 0.09(10) -1.5 0.36 *
	83.85	722.14		0.42(17)	0.26(20)	0^+ 1^+ 2^+ 3^+ 4^+	2^+	* -0.75 $0.12^{+4.30}_{-0.31}$ 4.92 *

unobserved intervening transition with energy 8.6 keV. There may exist another 27-keV γ ray as a decay from the 55-keV to the 27-keV level to have balanced incoming and outgoing intensity ratios at the 55-keV level.

The only excited state that has neither a direct nor an indirect coincidence relation in the proposed level scheme

is the 566-keV level with a relatively strong (127 on a scale of 1000) single decay to the ground state.

It is worth noting that, although we also detected the same transition cascades as found in former studies [7], the ordering of the transitions differs in our work. Consequently, some of the previously established levels are

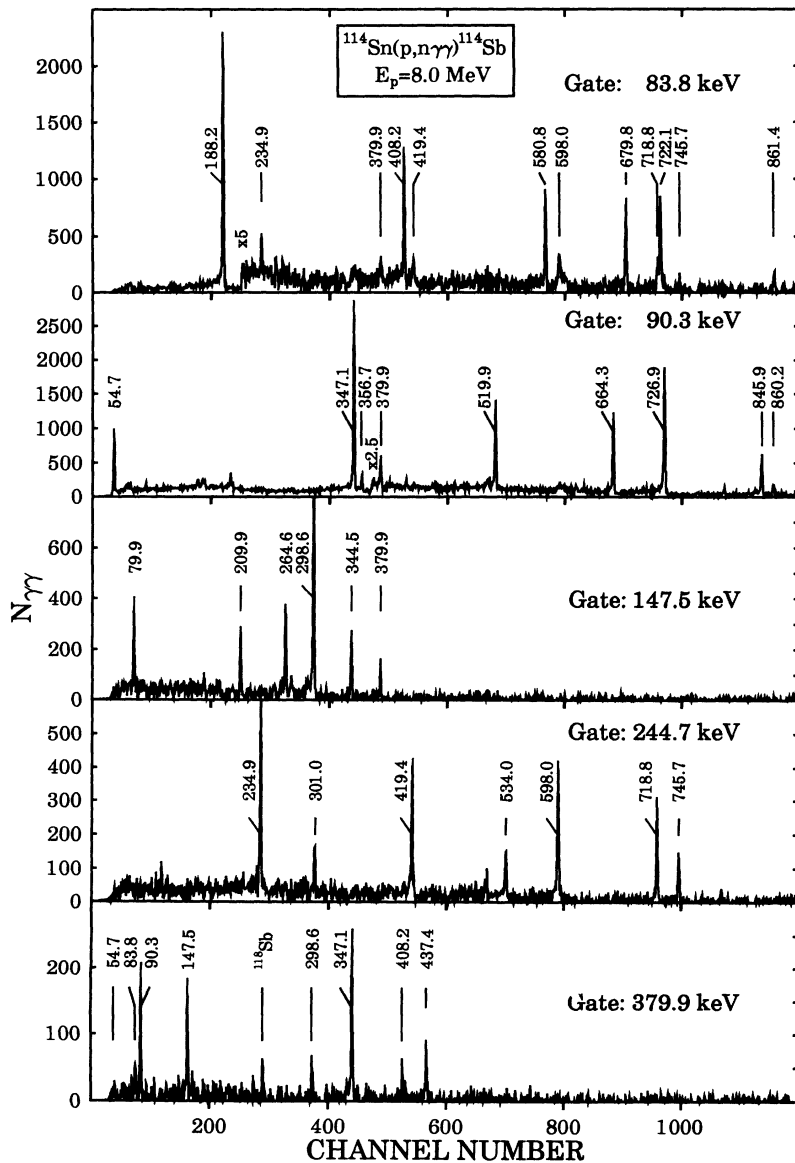


FIG. 3. Typical $\gamma\gamma$ -coincidence spectra. The background was subtracted.

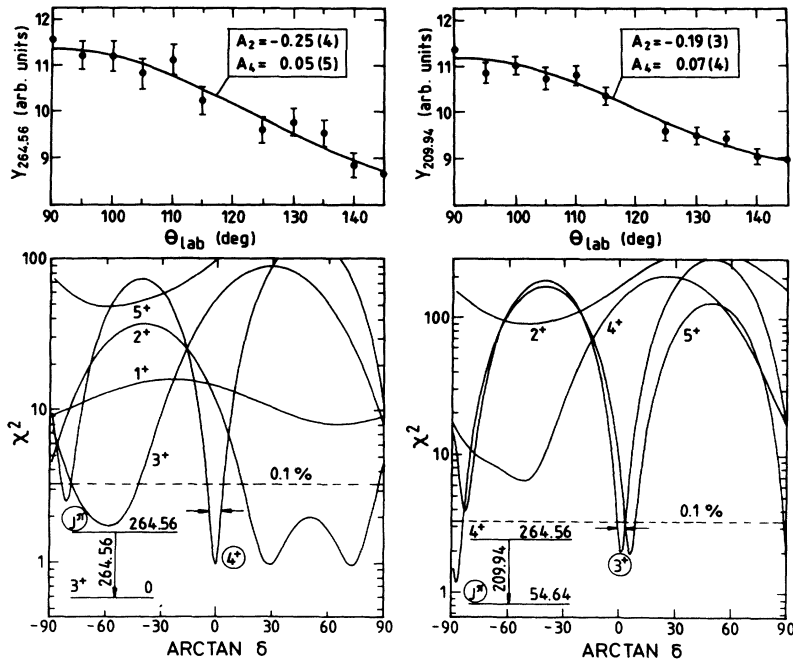


FIG. 4. The angular distribution of the 209-keV and 264-keV γ rays, as well as the reduced χ^2 fits of the theoretical distribution to the experimental ones as a function of $\arctan \delta$, where δ^2 is the $E2/M1$ intensity ratio for the transition. Labeled numbers are the assumed spins and parities for the state in question. Encircled numbers are adopted spins and parities based on all available data. The dashed lines show the 0.1% confidence limit for the reduced χ^2 .

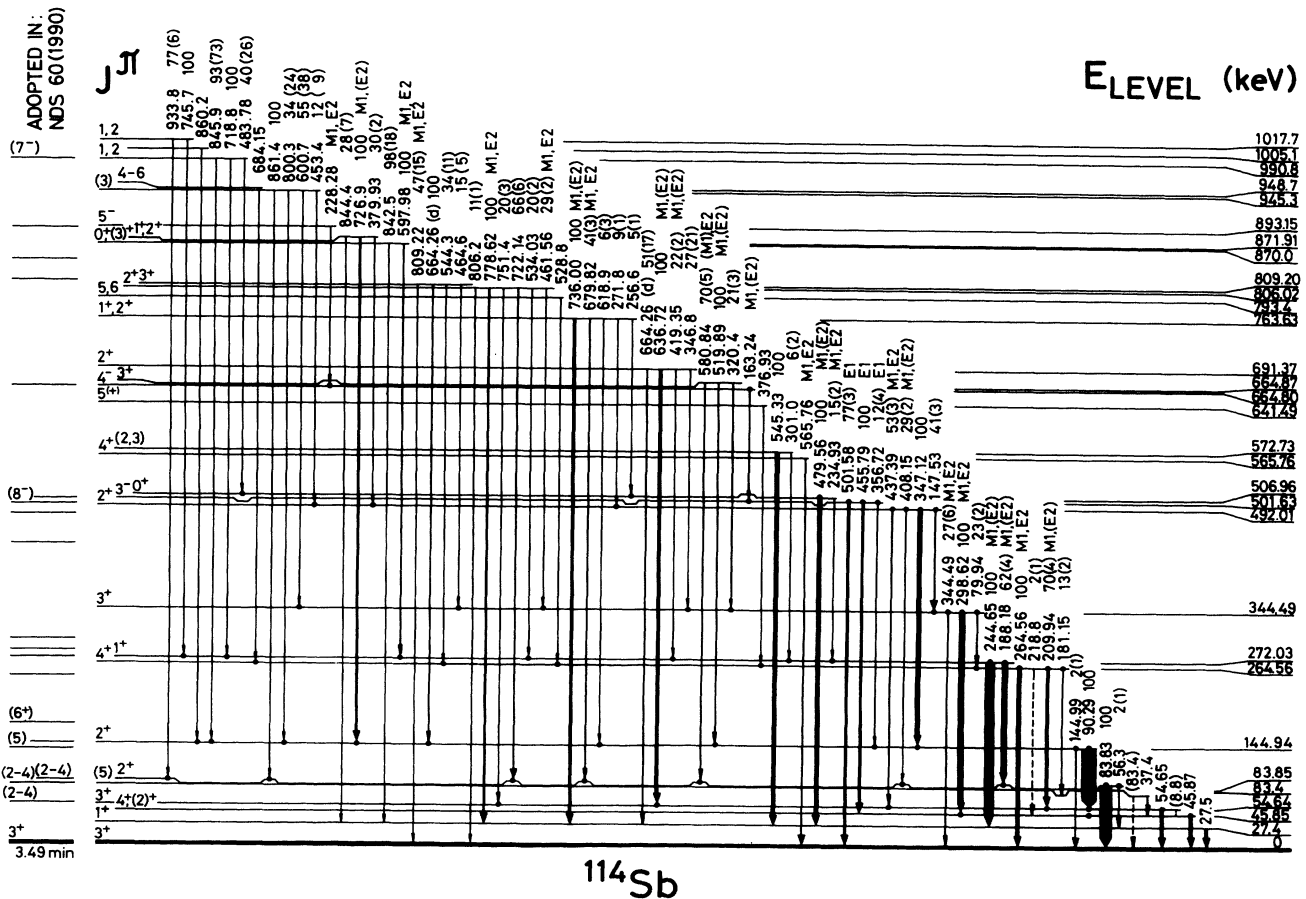


FIG. 5. Proposed level scheme of ^{114}Sb from $(p, n\gamma)$ reaction. Solid circles at the ends of arrows indicate $\gamma\gamma$ -coincidence relations. γ -branching ratios and multiplicities are also given. d denotes double placement. The 8.8-keV and 83.4-keV transitions were not observed; their energy values have been inferred.

TABLE III. Optical model parameters used in this work. The V , W , and $V_{s.o.}$ potential depths are given in MeV and the r range and a diffuseness parameters are in fm. E is the energy of the bombarding proton or outgoing neutron, given in MeV.

	V	W	$V_{s.o.}$	r_{real}	$r_{\text{imag.}}$	a_{real}	$4 a_{\text{imag.}}$
$p+^{114}\text{Sn}$	$66.10-1.13E$	13	7.5	1.25	1.25	0.65	0.47
$n+^{114}\text{Sb}$	$47.01-0.267E-0.0018E^2$	$9.52-0.053E$	7.5	1.28	1.24	0.66	0.48

rejected and others are proposed. The additional coincidence relations, internal conversion coefficients, and branching ratios of this work make us believe that the proposed levels are now correctly established.

A. Hauser-Feshbach analysis

As a result of detailed γ - and $\gamma\gamma$ -spectroscopic measurements, the low-spin, low-energy ($E_{\text{lev}} \leq 900$ keV) level scheme of ^{114}Sb can be considered nearly complete. Thus the cross sections for the neutron groups feeding the different ^{114}Sb levels can be deduced from internal transition intensities.

The $\sigma_{\text{lev}}(p, n)$ relative cross sections obtained this way are shown in Fig. 6. The internal conversion coefficients of the γ rays deexciting the levels below 200 keV are not known, and due to the low energy of these transitions, the majority of the transition intensities is furnished by conversion processes. Consequently, the neutron cross sections for these levels cannot be deduced precisely enough from the γ -ray intensities, and so the levels below 200 keV were ignored from the analysis.

Hauser-Feshbach theoretical results have been calculated at 7.8 MeV bombarding proton energy with the CINDY [13] program, which was based on the compound reaction model. The transmission coefficients were calculated using the optical model parameter set of Wilmore and Hodgson [15] for neutrons and that of Perey [16] (modified by Gyarmati *et al.* [17]) for protons. The parameters of the optical potentials are given in Table III. Beside the neutron channels, some (p, p') channels were also included. The experimental and theoretical cross sections were normalized at the 501.63-keV 3^- state because the spin for this level was uniquely determined by the multipolarity of transitions. In calculations of the theoretical curves, the values of the cross sections are

interdependent, since changing the spin of any individual level requires the redistribution of the outgoing flux through all the other channels. Nevertheless, the variation of the spin and parity of one level can cause only a 5–10% change in the cross sections of the others. This means that using only the Hauser-Feshbach analysis we cannot make a distinction between spins 1 and 2 or between spins 0 and 3, and the analysis is not sensitive to the parity.

B. Spin and parity assignment

The level spin assignments are based on the measured internal conversion coefficients of transitions, on the Hauser-Feshbach analysis, and on the γ -ray angular distribution results. The parities came exclusively from the multipolarity measurement. We used a multi-step approximation to assign spin and parity values to the levels. In the first step we determined the spins and parities of higher-lying states having ground state transitions, as only the spin of the ground state was previously known. Using then the multipolarity and angular distribution data for transitions from these higher-lying states we could determine the spins and parities of the low-lying states, too. Finally we determined the spin and parity values for the other higher-lying states. The arguments critical for the spin and parity assignment are summarized in Table IV.

V. PROTON-NEUTRON MULTIPLET STATES, PARABOLIC RULE CALCULATIONS

In the $^{114}_{51}\text{Sb}_{63}$ nucleus we may expect excitations of the odd proton and odd neutron, and the angular momentum coupling of different excited states. In a zeroth-order

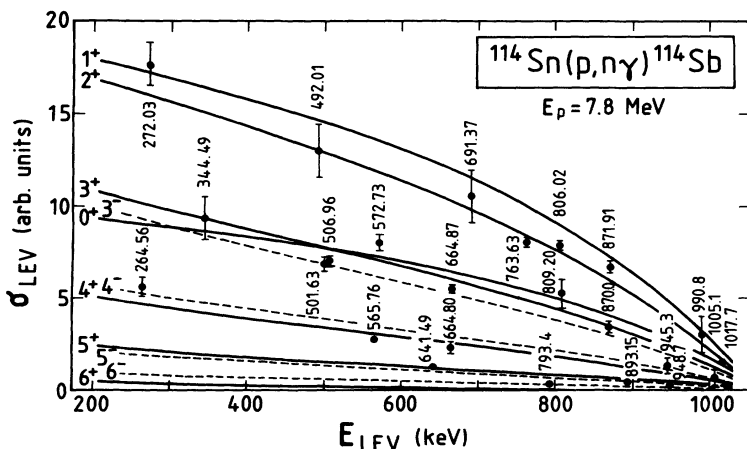


FIG. 6. Experimental relative cross sections (σ_{lev}) of the $^{114}\text{Sn}(p, n\gamma)^{114}\text{Sb}$ reaction as a function of the ^{114}Sb level energy (E_{lev}) at 7.8 MeV bombarding proton energy. The solid and dashed curves show Hauser-Feshbach theoretical results.

TABLE IV. Spin and parity assignments to ^{114}Sb levels.

E^* (keV)	J^π	Basis of J^π assignment
0	3^+	$\log ft < 6$ in β^+ decay to ^{114}Sn 2^+ and 4^+ levels [7]; measured magnetic moment and additivity rule calculations [6]
27.4	1^+	$M1, (E2)$ transitions from 0^+ and 2^+ states; angular distribution of the 244.7- and 778.6-keV γ rays prefer 1^+ final state
45.85	$4^+, (2)^+$	$M1, E2$ transition from 3^+ state; $E1$ transition from 3^- state; angular distribution of the 501-keV transition prefers 2^+ and 4^+ final states; no decay from low-spin states
54.64	3^+	$M1, (E2)$ transitions from 2^+ and 4^+ states; angular distribution of the 209.9-keV transition prefers 3^+ and 5^+ final states
83.4	(5)	decay to and from 4^+ states; decay from (6^+) in [3,4]
83.85	2^+	$M1, (E2)$ transitions from $1^+, 2^+, 3^+$ states
144.94	2^+	$M1, (E2)$ transitions from $1, 2^+$ and 3^+ states; $E1$ transition from 3^- state; angular distribution of the 347.1- and 519.9-keV γ rays prefers 2^+ final state
264.56	4^+	Hauser-Feshbach analysis gives 4; $M1, (E2)$ transition to 3^+ state; angular distribution of the 264.6-keV γ ray prefers 4^+
272.03	1^+	Hauser-Feshbach analysis gives 1, 2; $M1, (E2)$ transitions to $1, 2^+$ states; angular distribution of the 419.4-keV ray gives 1^+
344.49	3^+	Hauser-Feshbach analysis gives 0, 3; $M1, E2$ transitions to $3^+, 4^+$ states; $M1, E2$ transition from 2^+ state
492.01	2^+	Hauser-Feshbach analysis gives 1, 2; $M1, E2$ transitions to 2^+ and 3^+ states; angular distribution of the 347.1- and 437.4-keV γ rays prefer 2^+
501.63	3^-	$E1$ transitions to $2^+, 3^+, 4^+$ states
506.96	0^+	Hauser-Feshbach analysis gives 0, 3; $M1, (E2)$ transitions to 1^+ states.
565.76	4^+	Hauser-Feshbach analysis gives 4; $M1, E2$ transition to 3^+
572.73	(2,3)	Hauser-Feshbach analysis gives 0, 3; angular distribution of the 545.3-keV transition prefers 2
641.49	$5^{(+)}$	Hauser-Feshbach analysis gives 5; decay to 4^+
664.80	4^-	Hauser-Feshbach analysis gives 4; $M1, (E2)$ transition to 3^- ; angular distribution of the 163.2-keV γ ray prefers 4^-
664.87	3^+	Hauser-Feshbach analysis gives 0, 3; $M1, (E2)$ transition to 2^+ ; decay to 3^+
691.37	2^+	Hauser-Feshbach analysis gives 1, 2; $M1, (E2)$ transition to 3^+ state
763.63	$1, 2^+$	Hauser-Feshbach analysis gives 1, 2; $M1, (E2)$ transition to 1^+ , and $M1, E2$ transition to 2^+ states
793.4	5,6	Hauser-Feshbach analysis gives 5, 6; decay to 4^+
806.02	2^+	Hauser-Feshbach analysis gives 1, 2; $M1, E2$ transition to 3^+ ; angular distribution of the 722.1-keV γ ray prefers 2^+
809.20	3^+	Hauser-Feshbach analysis gives 0, 3; $M1, E2$ transition to 3^+
870.0	0^+	Hauser-Feshbach analysis gives 0, 3; $M1, E2$ transition to 1^+ state; decay only to 1^+ states
871.91	$1, 2^+$	Hauser-Feshbach analysis gives 1, 2; $M1, (E2)$ transition 2^+ state
893.15	5^-	Hauser-Feshbach analysis gives 5; $M1, E2$ transition to 4^-
945.3	(3)	Hauser-Feshbach analysis gives 3-5; transition to 2^+
948.7	4-6	Hauser-Feshbach analysis gives 4-6; decay to 4^+
990.8	1,2	Hauser-Feshbach analysis gives 0-3; decay to $0^+, 1^+, 2^+$ states
1017.7	1,2	Hauser-Feshbach analysis gives 0-3; decay to 1^+ and 2^+ states

approximation the energy of the p - n multiplet can be obtained by the addition of energies of the odd proton and odd neutron states.

The low-lying states of the neighboring ^{113}Sb and $^{113}\text{Sn}_{63}$ [18] are shown in Fig. 7(a). The $5/2^+$ ground and the 814-keV excited $7/2^+$ states of ^{113}Sb have dominant $\pi d_{5/2}$ and $\pi g_{7/2}$ configurations, while the other states have rather strong collective phonon components [19]. The low-lying states of ^{113}Sn (presumably neutron excitations) with $1/2^+, 7/2^+, 5/2^+, 3/2^+$, and $11/2^-$ spins at 0, 77, 410, 498, and 738 keV excitation energies have $\nu s_{1/2}, \nu g_{7/2}, \nu d_{5/2}, \nu d_{3/2}$, and $\nu h_{11/2}$ character, respectively [20]. The one-phonon states are expected above 1 MeV in the ^{113}Sn nucleus.

According to Fig. 7(a), the lowest-lying states of ^{114}Sb are expected to be members of the proton-neutron multi-

plets predominantly based on the $\pi d_{5/2}$ proton configuration. To estimate the splitting of the different multiplets we performed a parabolic rule [21] calculation. The calculations were performed in a way similar to those for ^{112}In [22], using the same formulas.

The parameters of the calculations were as follows: The strength of the quadrupole core polarization interaction, calculated on the basis of particle-vibration coupling theory, using the formula given in Ref. [21], was $\alpha_2^0=4.2$ MeV; the strength of the spin polarization interaction, $\alpha_1^0 \approx 15/A=0.13$ MeV. These values are very close to those used in the interpretation of the level scheme of the ^{118}Sb [23]. The occupation probabilities of quasineutron states were calculated in a BCS approximation using the single-particle energies and pairing interaction strength of Kisslinger and Sorensen [24].

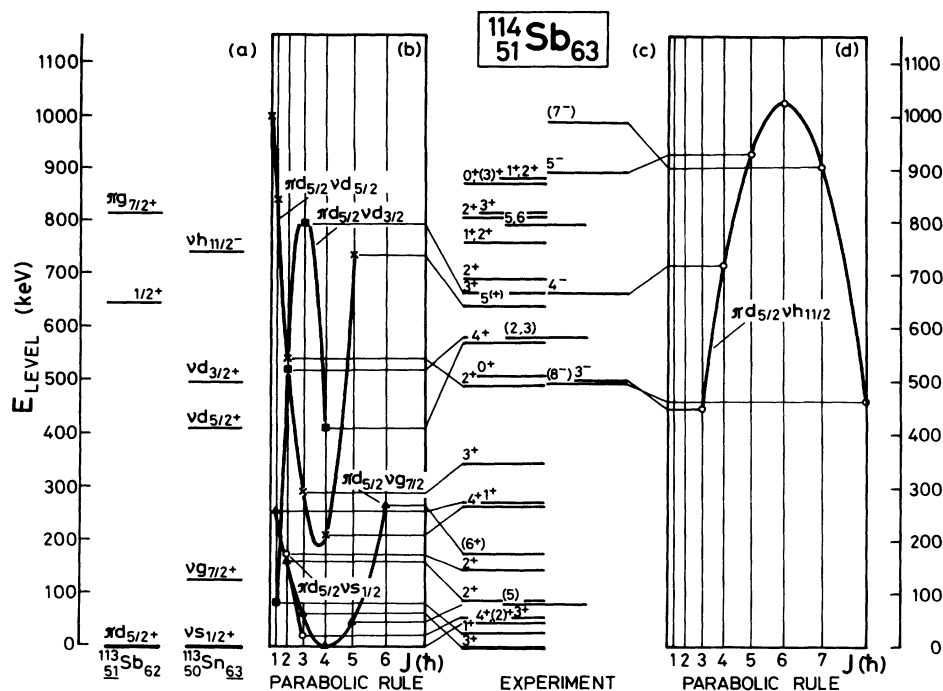


FIG. 7. Proton-neutron multiplet states in ^{114}Sb . (a) Experimental level energies and configurations of the lowest-lying states of ^{113}Sb and ^{113}Sn . (b) and (d) Results of the parabolic rule calculations for positive- and negative-parity states. The abscissa is scaled according to $J(J+1)$, where J is the spin of the state. (c) Experimental results on ^{114}Sb levels.

They are as follows: $V^2(\nu d_{3/2})=0.091$, $V^2(\nu d_{5/2})=0.836$, $V^2(\nu g_{7/2})=0.671$, $V^2(\nu h_{11/2})=0.119$.

The result of the calculations are presented in Fig. 7(b) for the positive-parity states and in part (d) of the figure for the negative-parity states. As in the case of other parabolic rule calculations, we used one overall normalization term, which pushed up all the members of the multiplets with the same energy.

The levels determined from our measurements are presented in Fig. 7(c). The three states shown with $J \geq 6$ were adopted from Ref. [7]. The experimental states could be associated with the calculated ones on the basis of the energies and spins, and the dominant decay mode, since in the quasiparticle shell model strong (≈ 1 Weisskopf unit) $M1$ transitions are expected between the J and $J \pm 1$ members of the multiplets. The dominant decay mode was determined by rescaling the branching ratios of the non- $E2$ transitions with E_γ^3 .

The $\pi d_{5/2} \nu g_{7/2}$ multiplet. The configuration of the ground state is $\pi d_{5/2} \nu g_{7/2}$ according to the magnetic moment measurement [6]. On the low-spin side the 188–84-keV gamma cascade decays into the ground state, indicating that the 272-keV 1^+ and the 84-keV 2^+ states are the 1^+ and 2^+ members of the ground state multiplet. The presence of the relatively strong 244-keV transition shows that the first two 1^+ states are mixed. On the high-spin side the ground state is favored by the 90–37–46-keV cascade, suggesting that the 174-keV 6^+ , the 83-keV 5^+ , and the 46-keV 4^+ states form the high-spin part of the multiplet.

The $\pi d_{5/2} \nu s_{1/2}$ doublet is expected to be the ground state multiplet in the zeroth-order approximation, but due to a somewhat larger splitting of the $\pi d_{5/2} \nu g_{7/2}$ multiplet, it became an excited multiplet. The members of the doublet are connected with the strong 90-keV gamma transition.

The $\pi d_{5/2} \nu d_{5/2}$ multiplet. The lowest-lying state of this multiplet is the 265-keV 4^+ state. It is chosen by the 147–80-keV gamma cascade; consequently the 2^+ and 3^+ members of the multiplet may be the 34- and 492-keV states, respectively. The 5^+ member of the multiplet may be the 641-keV 5 state.

The $\pi d_{5/2} \nu d_{3/2}$ multiplet. The intruding 1^+ state at 27 keV may originate from this multiplet. The possible 2^+ member of the multiplet is the 572-keV (2,3) state, which is strongly connected to the 665-keV 3^+ state, the probable 3^+ member of the multiplet. The 4^+ member of this multiplet may be 566-keV 4^+ state. Unfortunately the intermultiplet transition from the 3^+ state is missing, but it might be a bit weaker than the 92-keV transition and hence not seen in the present experimental circumstances.

The $\pi d_{5/2} \nu h_{11/2}$ multiplet is the lowest-lying negative-parity multiplet. The 501-keV 3^- , 665-keV 4^- , and the 893-keV 5^- states connected by the 228–163-keV cascade of gamma transitions form the low-spin part of the multiplet. The high-spin 8^- and 7^- members of the multiplet were observed in heavy ion reactions [3,4].

Up to 700 keV all but two states were identified as quasiparticle state, using the parabolic rule. The two unidentified states are expected to arise from one-phonon multiplets.

ACKNOWLEDGMENTS

We are indebted to Prof. T. Fényes for useful discussions. The assistance in experiments of the cyclotron staff, as well as of the members of the cryogenic laboratory is recognized. We are indebted also to Dr. J. Gulyás, Dr. S. Mészáros, and Dr. A. Valek for their help in the measurements. This work was supported in part by the Hungarian Scientific Research Foundation (OTKA) Contract No. 3004.

- [1] M. E. J. Wigmans, R. J. Heynis, P. M. A. van der Kam, and H. Verheul, *Phys. Rev. C* **14**, 243 (1976).
- [2] R. Kamermans, H. W. Jongsma, T. J. Ketel, R. van der Wey, and H. Verheul, *Nucl. Phys.* **A266**, 346 (1976).
- [3] P. van Nes, W. H. A. Hesselink, W. H. Dickhoff, J. J. van Ruyven, M. J. A. de Voigt, and H. Verheul, *Nucl. Phys.* **A379**, 35 (1982).
- [4] R. Duffait, J. van Maldeghem, A. Charvet, J. Sau, K. Heyde, A. Emsallem, M. Meyer, R. Beraud, J. Treherne, and J. Genevey, *Z. Phys. A* **307**, 259 (1982).
- [5] C. Gil, K. Nishiyama, T. Nomura, T. Yamazaki, and K. Miyano, *J. Phys. Soc. Jpn.* **34**, 874 (1973).
- [6] B. E. Zimmerman, W. B. Walters, P. F. Mantica, Jr., H. K. Carter, M. G. Booth, J. Rikovska, and N. J. Stone, *Hyperfine Interact.* **75**, 117 (1993).
- [7] J. Blachot and G. Marguier, *Nucl. Data Sheets* **60**, 139 (1990).
- [8] W. F. van Gunsteren, K. Allart, and E. Boeker, *Nucl. Phys.* **A266**, 365 (1976).
- [9] Z. Árvay, T. Fényes, K. Füle, T. Kibédi, S. László, Z. Máté, Gy. Móri, D. Novák, and F. Tárkányi, *Nucl. Instrum. Methods* **178**, 85 (1980); T. Kibédi, Z. Gácsi, A. Krasznahorkay, and S. Nagy, *ATOMKI Annual Report*, Debrecen, 1986, p. 55; T. Kibédi, Z. Gácsi, and A. Krasznahorkay, *ATOMKI Annual Report*, Debrecen, 1987, p. 100.
- [10] Z. Gácsi, T. Fényes, and Zs. Dombrádi, *Phys. Rev. C* **44**, 626 (1991).
- [11] J. Blachot and G. Marguier, *Nucl. Data Sheets* **59**, 333 (1990); *Table of Isotopes*, 7th ed., edited by C. M. Lederer and V. S. Shirley (Wiley, New York, 1978).
- [12] H. Helppi, University of Jyväskylä, JYFL Report No. 1/1976, 1976.
- [13] E. Sheldon and V. C. Rogers, *Comput. Phys. Commun.* **6**, 99 (1973).
- [14] G. Székely, *Comput. Phys. Commun.* **34**, 313 (1985).
- [15] D. Wilmore and P. E. Hodgson, *Nucl. Phys.* **55**, 673 (1964).
- [16] F. G. Perey, *Phys. Rev.* **131**, 745 (1963).
- [17] B. Gyarmati, T. Vertse, L. Zolnai, A. I. Barishnikov, A. F. Gurbich, N. N. Titarenko, and E. L. Yadrovsky, *J. Phys. G* **5**, 1225 (1979).
- [18] J. Lyttkeis, K. Wilson, and L. P. Ekström, *Nucl. Data Sheets* **33**, 1 (1981).
- [19] A. G. De Pinho and J. M. F. Jeronymo, *Nucl. Phys.* **A116**, 408 (1968).
- [20] G. Ch. Madueme, L. O. Edwardson, and L. Westenberg, *Phys. Scr.* **13**, 17 (1976).
- [21] V. Paar, *Nucl. Phys.* **A331**, 16 (1979).
- [22] T. Kibédi, Zs. Dombrádi, T. Fényes, A. Krasznahorkay, J. Tímár, Z. Gácsi, A. Passoja, V. Paar, and D. Vretenar, *Phys. Rev. C* **37**, 2391 (1988).
- [23] J. Gulyás, T. Fényes, M. F. F. M. Hassan, and Zs. Dombrádi, *Phys. Rev. C* **46**, 1218 (1992).
- [24] L. S. Kisslinger and R. A. Sorensen, *Rev. Mod. Phys.* **35**, 853 (1963).